Experimental Study on the Effect of Chevrons on Flow Separation in Rocket Nozzles

Ralf Stark, Carla Rieping

German Aerospace Center, D-74239 Lampoldshausen, Germany, Email: ralf.stark@dlr.de

Thomas Aichner, Stefan Köglmeier and Manuel Frey

ArianeGroup, D-82024 Taufkirchen, Germany

KEYWORDS: rocket nozzle, flow separation, side load

ABSTRACT:

During the transient start-up and shut-down of rocket engines, the supersonic flow inside the divergent section of the rocket nozzle separates, causing undesired side loads.

An experimental test campaign was conducted to study the effect of chevrons on the flow separation in rocket nozzles, and thus a potential side load reduction. Positive results were obtained and are presented here.

1. INTRODUCTION

The convergent-divergent nozzle is the part of the rocket engine that expands the hot, highly pressurized combustion gases (T_{cc}, p_{cc}) and accelerates them to a high speed, namely supersonic speed (u_e). Depending on the area ratio (A_e/A_t) of the nozzle and the respective nozzle pressure ratio (NPR = p_{cc}/p_e), the flow can be over-expanded below ambient pressure ($p_e < p_a$). However, the flow can be over-expanded only to a certain point. If the overexpansion is too strong, the boundary layer detaches and ambient air is sucked into the remaining separated backflow region of the nozzle (Fig. 1). For a given nozzle geometry, the position of the flow separation is a function of the local gas properties, the NPR, and the related Mach number M_{sep} [1, 2].

The flow separation itself fluctuates and forms a separation zone ($X_{sep} \rightarrow X_p$ in Fig. 1) that is also asymmetrically distributed in the circumferential direction. This, in combination with comparatively low-pressure fluctuations of the attached upstream flow (caused by combustion) and significant pressure fluctuations in the downstream separated backflow region, causes a dynamic side load force. These undesired side loads stress not only the nozzle itself, but also the rocket engine, the rocket structure and the payload. Hence, understanding flow separation and ways to reduce the related lateral force are crucial for rocket engine design.

The presented experimental study investigated the impact of sawtooth like chevrons, protruding circumferentially into the flow at the nozzle exit, on the flow separation, and consequently on side load reduction.

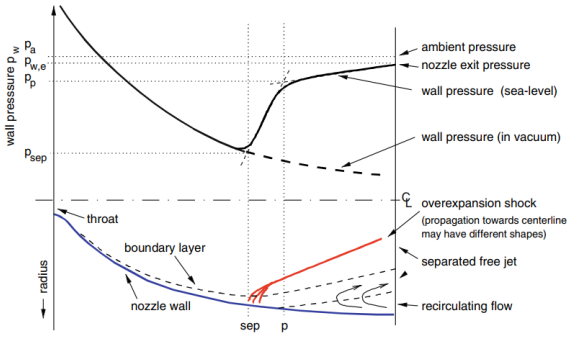

Figure 1. Flow separation in a strongly over-expanding rocket nozzle [3].

2. EXPERIMENTAL SETUP

The study was conducted at DLR's cold flow subscale test facility P6.2 in Lampoldshausen using dry gaseous nitrogen as working fluid, which was stored in 20 MPa high pressure vessels under ambient temperature. Nitrogen was used instead of air to minimize condensation effects. A supply system, consisting of an automatic valve, a particle filter, a pressure reducer, a regulation valve, and a mass flow meter, connected the storage vessels with a settling chamber that was mounted on a horizontal rig. This settling chamber was equipped with a set of grids and honeycombs to homogenize the flow. The facility featured a maximum total pressure of p_0 = 6 MPa, with a maximum mass flow of 4.2 kg/s.

To study the interaction of a subscale rocket nozzle with an additional chevron ring, the already tested TICTOP B1 nozzle was chosen. The TICTOP B1 combined the internal shock free throat section of a truncated ideal contour nozzle (TIC) with a thrust optimized parabola nozzle extension (TOP) [4, 5]. It was made of acrylic glass, with a wall thickness of 8 mm (Fig. 2).

The chevron ring was laser-cut from a 1 mm aluminum sheet. It featured 90 chevrons directed inwards, with a height of 7 mm and a tooth root width of 2 mm each. The ring was mounted either directly at the nozzle exit or with a chevron mounting distance of CMD = 7.2 mm.

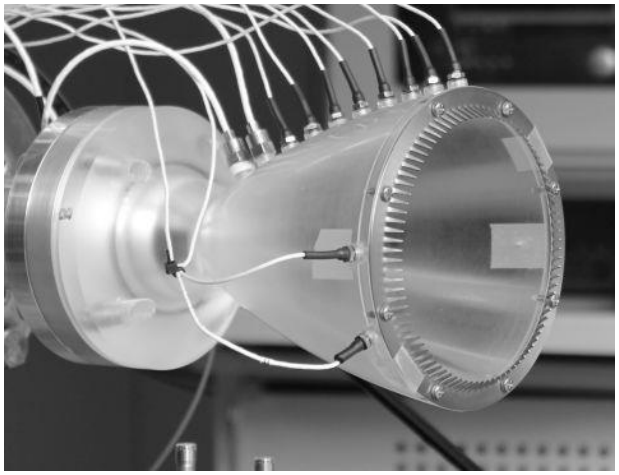

Figure 2. TICTOP B1 subscale nozzle with chevrons (directly mounted).

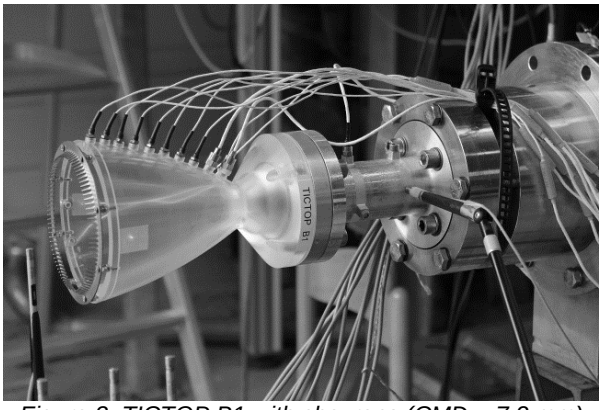

Figure 3. TICTOP B1 with chevrons (CMD = 7.2 mm) and capacitive displacement sensor near bending tube.

To measure the static wall pressure distribution, the nozzle was equipped with an axial row of 10 piezoresistive XT-154-190M type Kulite pressure transducers, directly mounted into the nozzle wall. Two additional transducers, mounted in a cross section near the nozzle exit at different circumferential positions, completed the wall pressure measurements. All transducers were connected to the flow via orifices (0.5 mm), drilled perpendicularly into the nozzle wall. The transducers had a measurement range of 0.1 MPa with an accuracy of 0.5 % relative to the upper range limit. The natural frequency of the transducers' pressure-sensitive semiconductor membrane was higher than 50 kHz. However due to the eigenfrequency of the combination of orifice and cavity, the pressure signals were analogue filtered with a cut-off frequency of 8 kHz and recorded with a high frequency rate of 25 kHz.

The generated side loads were measured using a Micro-Epsilon capaNCDT 6500 system with a DL6530 demodulator, and a CSH05-Cam1,4 capacitive sensor. The sensor, featuring a measuring range of 500 µm (50 µm/V) with a linearity deviation of ±0.09 %, was used to determine the horizontal displacement of the bending tube (Fig. 3). The measurement signals were recorded with a sampling frequency of 65.5 kHz and a high pass filter of 25 Hz.

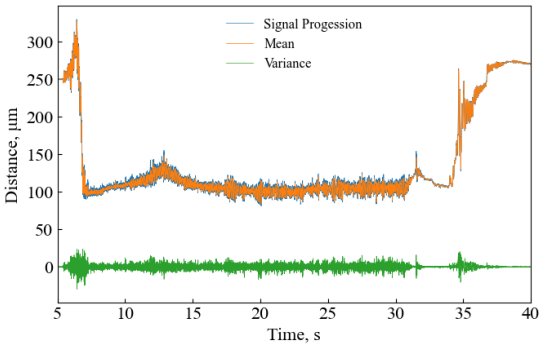

Figure 4. Example of signal decomposition.

Compared to the unpressurized initial state, the bending tube stiffened during the test run due to the increasing internal pressure, and the nozzle moved slightly upwards. This leads to a drift of the obtained displacement measurement signal (Fig. 4). The decomposition of the mean and variable components made it possible to evaluate the side load dynamics.

The test setup was temporarily completed by a horizontally mounted guide tube. The guide tube GT-Ref, in combination with the TICTOP B1 nozzle, was a geometrical downscaling of a typical rocket engine test bench configuration [6]. Figure 5 illustrates the geometrical proportions. The effect of the different specific heat ratios of hot and cold flow exhaust jets was not considered.

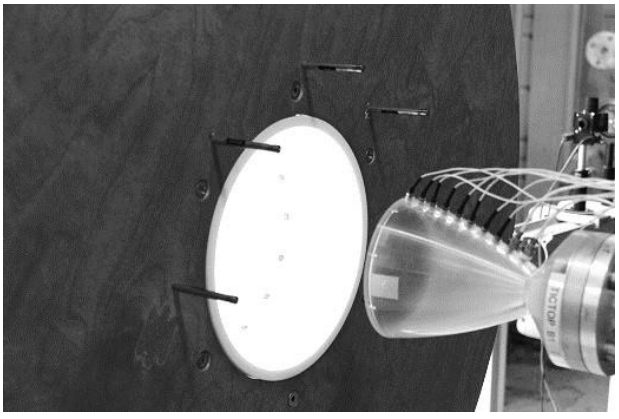

Figure 5. GT-Ref with circular plate.

The guide tube was made of polyamide (PA12) and directly printed in 3D by selective laser sintering (SLS). Its design included plate mounts and sliders. The sliders enabled a horizontal adjustment of the guide tube with regard to the nozzle exit. The experimental setup was completed by a circular plate

around the guide tube inlet, representing a test cell floor, in order to mimic the inflow conditions of the full-scale guide tube.

For comparison reasons, all configurations were tested with the same test sequence. Figure 6 illustrates the related total pressure profile. A steep total pressure increase was followed by a medium gradient phase, where the smooth downstream shift of the flow separation was recorded. To study the behavior of the full-flowing nozzle, a pressure plateau completed the sequence, until the nozzle was shut down by closing all valves with maximum speed.

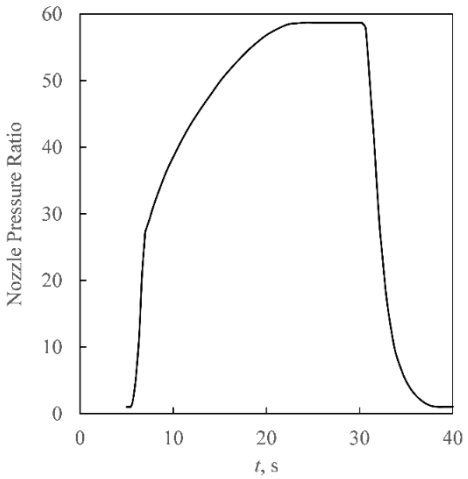

Figure 6. Test Sequence.

3. RESULTS AND DISCUSSION

Experimental studies have shown that the suction effect of downstream mounted guide tubes influenced the flow separation in rocket nozzles and shifted it downstream, towards the nozzle exit. Here, the strength of the effect was inversely proportional to the distance *d* between nozzle exit and guide tube inlet [7]. The question arose what effect chevrons mounted at the nozzle exit might have on the flow separation, as they were supposed to swirl the ambient air sucked into the separated backflow area, reducing its axial momentum.

Figure 7, top compares the NPR required to achieve an attached flow at a respective axial sensor position X/R_{th} for different configurations. Here, the red circles represent the flow separation behavior of the initial TICTOP B1 nozzle, without any chevrons or guide tube applied. All data points were averaged from several runs of the same configuration.

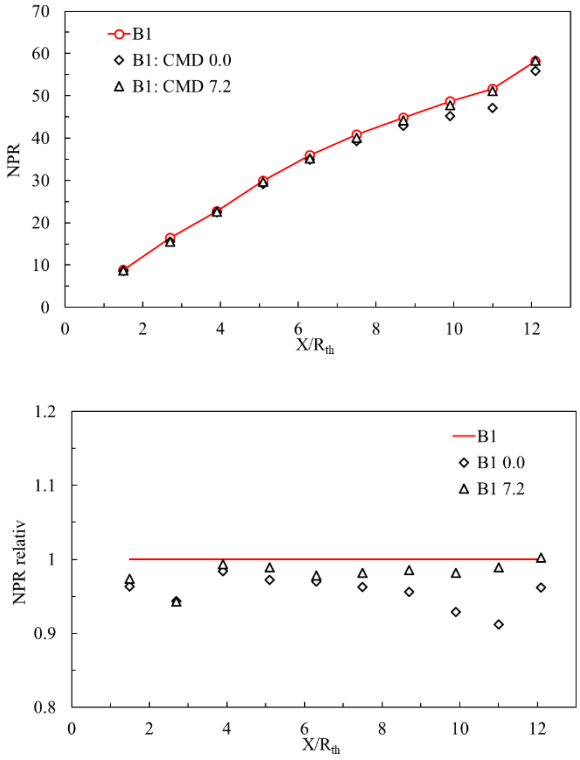

Figure 7. Impact of chevrons on flow separation (free jet).

Chevrons mounted directly at the nozzle exit (Fig. 2) revealed a reduced NPR, necessary to reach the respective sensor position (diamonds). This means that with the same NPR, the flow separation was shifted downstream. The effect was clearly visible in the rear section of the nozzle ($X/R_{th} > 8$). The relative comparison (Fig. 7, bottom) showed that there was also an impact for the remaining upstream nozzle section, albeit to a much lesser extent. All in all, an NPR reduction of up to 9% was achieved. Chevrons mounted with a distance of CMD = 7.2 mm at the nozzle exit using spacers (Fig. 3) showed a minor impact along the entire length of the nozzle (triangles).

The comparison of the two configurations led to the conclusion that the chevrons influenced the nozzle flow in two ways: by 1) their shape, i.e. their height, their number and the angle at which they protruded into the flow, and 2) their distance from the nozzle exit.

Combinations of nozzle B1, chevrons and the reference guide tube GT-Ref were also studied. Figure 8 shows the results obtained for a nozzle exit to guide tube inlet distance of 23% of the nozzle exit diameter ($d = 0.23 \cdot D_e$). First of all, the impact of the suction effect caused by the guide tube became apparent (orange stars). The flow separation position was shifted downstream over almost the entire NPR range.

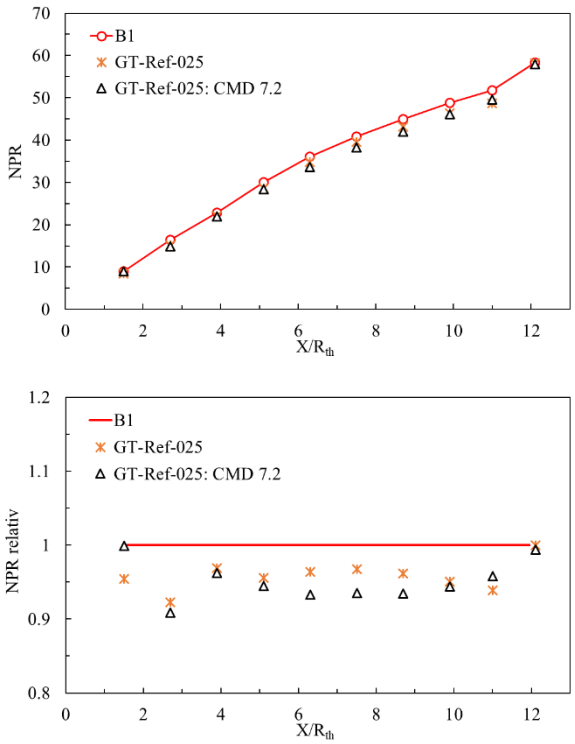

Figure 8. Chevrons and guide tube, d = 0.23·De.

Due to limited test facility availability, only chevrons mounted with a distance of CMD = 7.2 mm could be tested (triangles). Their impact on the separation in the middle nozzle section was clearly demonstrated ($5 < X/R_{th} < 10$).

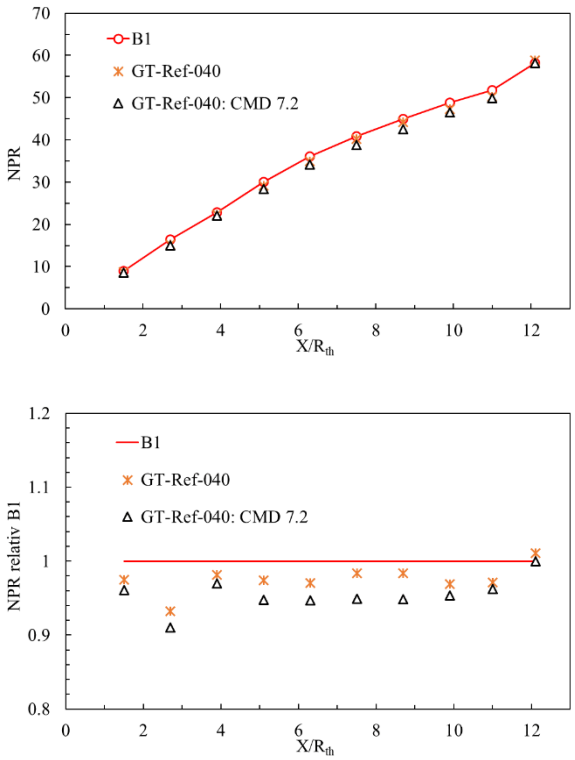

Figure 9. Chevrons and guide tube, d = 0.37·De.

Similar effects were found for a nozzle-to-guide-tube distance of $d = 0.37 \cdot D_e$ (Fig. 9). Not unexpectedly, due to the reduced suction effect, the guide tube's impact on the separation position shift decreased. However, the chevrons also had a comparable additional impact on the separation shift in the nozzle's middle section here (Fig. 9, bottom).

Unfortunately, the tight test campaign schedule did not allow to study nozzle-to-guide-tube distances representative for main stage rocket engine test facilities, i.e. $d > D_e$.

Previous experimental studies had shown that shifting the flow separation towards the nozzle exit significantly reduces the induced side loads [8, 9]. The question arose whether or not this also applies to the separation shift induced by the chevrons.

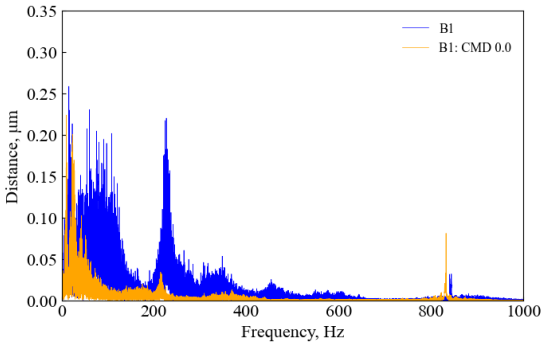

Figure 10. FFT of side load measurement signals, chevrons directly mounted.

Figure 10 gives the Fast Fourier Transformation (FFT) of the measured side loads of the initial B1 nozzle configuration (blue line), i.e. without the impact of a guide tube or a ring of chevrons.

In addition to a strong background noise below a frequency of 170 Hz, two distinct frequency peaks could be recognized. The 227 Hz peak was typical for flow separation induced side loads in rocket nozzles. The 840 Hz peak originated from the supply system. It was an eigenfrequency of the settling chamber upstream of the test specimen, which is already known from previous test campaigns. Figure 11, top shows an FFT of the total pressure in the settling chamber with the clearly visible peak of the eigenfrequency mentioned. An analysis according to Pearson's method showed the linear correlation between total pressure oscillation and the resulting side loads (Fig. 11, bottom). By damping the settling chamber appropriately, it was possible to eliminate the resonance in the subsequent test campaigns.

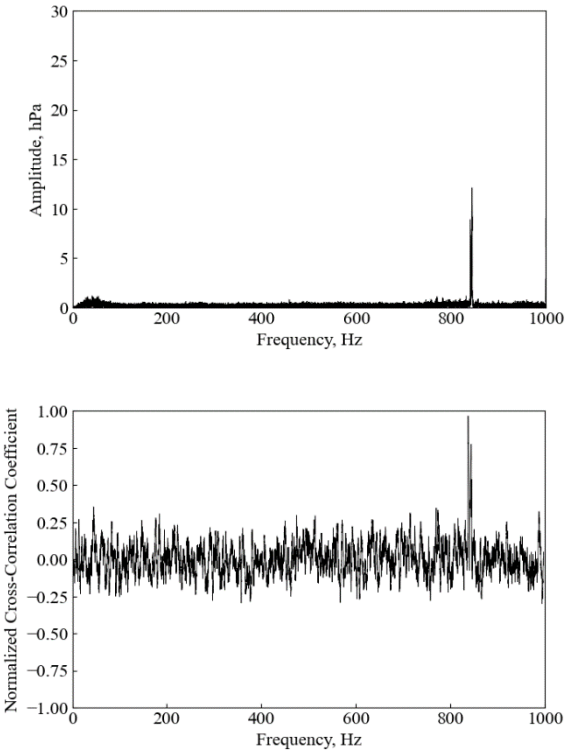

Figure 11. FFT of total pressure (top), correlation with side loads (bottom).

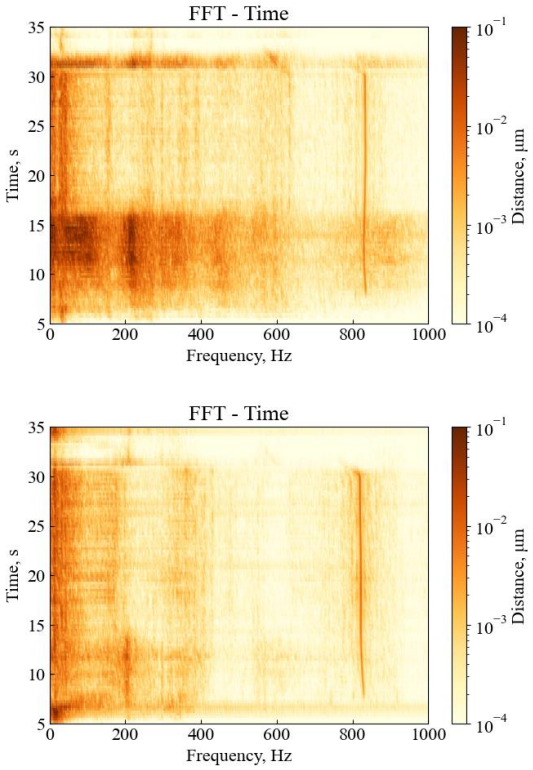

Figure 12. B1 side loads without (top) and with directly mounted chevrons (bottom).

Figure 10 also reveals the remarkable impact of the directly mounted chevrons on the side loads (orange line). Not only was the typical side load peak clearly reduced, but the background noise was also reduced significantly.

Due to the storage of the nitrogen outside of the test facility, its total temperature varied from test run to test run. This led to slightly different frequency peaks, e.g. 840 Hz → 835 Hz eigenfrequency of the settling chamber.

Figure 12, top displays the time course of B1's initial side loads in the frequency range. As expected, high side loads were induced during the medium NPR gradient start-up phase and the fast shut-down (see Fig. 6, test sequence). The full flowing nozzle showed only low side loads (t = 17→31 s). It became clear that the side loads induced by the settling chamber resonance were independent from the flow separation inside the nozzle (840 Hz peak).

In comparison, Fig. 12, bottom reveals the significant side load reduction over the entire test run, with chevrons directly mounted at the nozzle exit. Additionally, it could be observed that the full flowing state started earlier (t ~ 14 s).

Although their impact on the position of the flow separation was smaller, the chevrons mounted with a distance of 7.2 mm showed a comparable aspired reduction of the side loads (Fig. 13, orange line). The time course in the frequency range (Fig. 14) was very similar to that of the directly mounted chevrons. However, here an earlier full flowing state was not detected (t ~ 17 s).

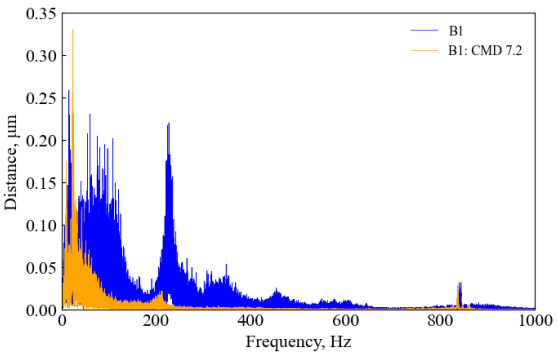

Figure 13. FFT of side load measurement signals, CMD = 7.2 mm.

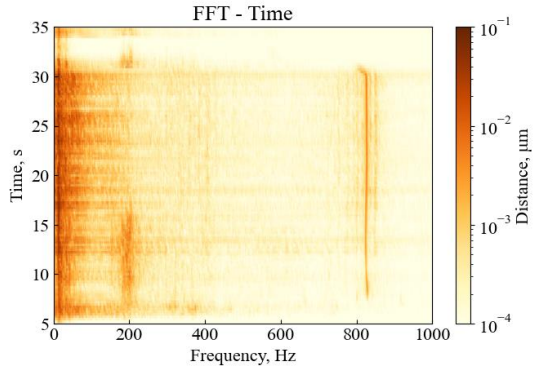

Figure 14. B1 side loads with CMD = 7.2 mm.

A comparable picture emerged for B1 combined with GT-Ref, e.g. for $d = 0.37 \cdot D_e$. Initially, the suction effect of the guide tube shifted the separation towards the nozzle exit and thus reduced the side loads as expected. This became clear in the FFT of the measured side load signal (Fig 15, blue line) as well as in its time course (Fig 16). Hence, with GT-Ref an earlier full flowing state was also achieved (t ~ 14 s).

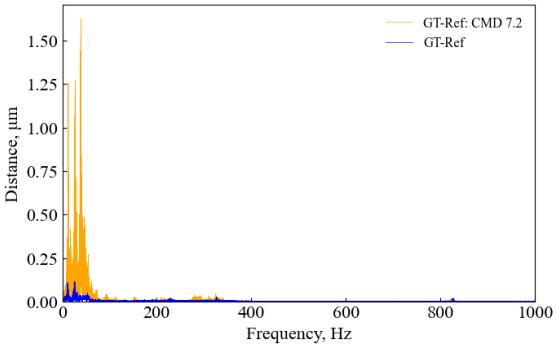

Figure 15. FFT of side load measurement signals. B1 combined with GT-Ref at $d = 0.37 \cdot D_e$, with and without chevrons, CMD = 7.2 mm.

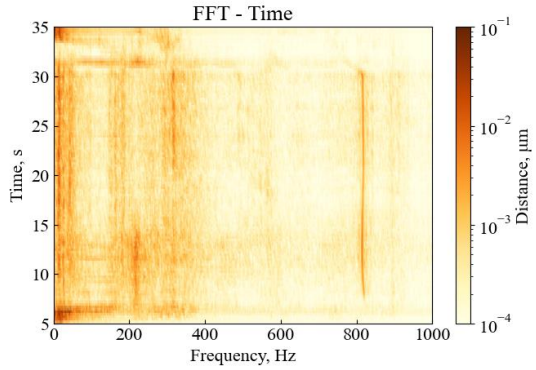

Figure 16. Side loads of B1 combined with GT-Ref at $d = 0.37 \cdot D_e$, without chevrons.

The negative impact of the chevrons added with CMD = 7.2 mm was completely unexpected, as an increased separation shift was also observed here (see Fig. 9, bottom). The FFT (Fig. 15, orange line) revealed a surprising side load noise for frequencies below 50 Hz. Like the settling chamber induced peak, the noise was independent from the nozzle flow state. There seemed to be another effect that superposed the behavior of the combination of nozzle and chevrons observed before. It is reasonable that the acoustic coupling of nozzle and guide tube was responsible here, which was at its maximum for a nozzle exit to guide tube inlet distance of $d = 0.5 \cdot D_e$ [6]. Distances above $d = 0.76 \cdot D_e$ were less critical. Beyond this value, it was shown that the suction effect of the guide tube almost disappeared [7]. It can be assumed that in real test facility or launch pad application ($d > D_e$), the positive effect of the chevrons on side load reduction predominates.

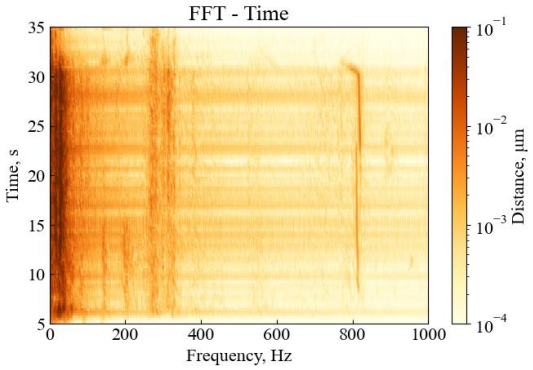

Figure 17. Side loads of B1 combined with GT-Ref at $d = 0.37 \cdot D_e$, with chevrons, CMD = 7.2 mm.

4. CONCLUSION

It has been shown that the chevrons shifted the separation position towards the nozzle exit, and hence decreased the induced side loads. Chevrons mounted directly at the nozzle exit and chevrons mounted with a gap revealed a comparable side load reduction. Unfortunately, the configurations with a guide tube were superimposed by strong acoustic couplings. In the case of realistic application scenarios, however, a side load reduction should be achieved.

5. ACKNOWLEDGEMENTS

The presented work was performed within the frame of the project grant “Technologien und Anwendungen für Raketenantriebssysteme 2020,” managed by the German Aerospace Center (DLR), support code 50RL1710.

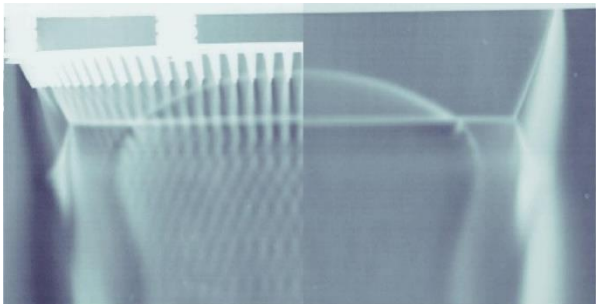

Figure 18. Schlieren image of full flowing B1's exhaust jet in X-Ray style, with (left) and without (right) chevrons impact on shear layer.

6. REFERENCES

1. Stark, R. (2013). Flow Separation in Rocket Nozzles – An Overview. AIAA-2013-3840, 49th AIAA/ASME/SAE/ASEE Joint Propulsion Conference.

2. Stark, R. & Wagner, B. (2009). Experimental study of boundary layer separation in truncated ideal contour nozzles. *Shock Waves* **19**(3), 185-191.

3. Hagemann, G. & Frey, M. (2008). Shock pattern in the plume of rocket nozzles: needs for design consideration. *Shock Waves* **17**(6), 387-395.

4. Frey, M., Makowka, K., Aichner, T., Stark, R. & Génin, C. (2017). The TICTOP nozzle - first experimental results. EUCASS, 7th European Conference for Aerospace Sciences, No. 359.

5. Stark, R. & Génin, C. (2017). Experimental Study of TICTOP Nozzles. 31st International Symposium on Shock Waves (ISSW31), No. 45.

6. Stark R., Wick C., General S., Möller C., Aichner T., Köglmeier S. & Frey M. (2023). Experimental Study of the Acoustical Interaction of a Subscale Rocket Nozzle Exhaust Jet and different Guide Tubes. *International Journal of Energetic Materials and Chemical Propulsion (IJEMCP),* **22**(4), 43-57.

7. Stark R., Rieping C. & Esch T. (2023). The Impact of Guide Tubes on Flow Separation in Rocket Nozzles. Aerospace Europe Conference 2023 / Joint 10th EUCASS – 9th CEAS Conference.

8. Stark, R. & Génin, C. (2016). Optimisation of a Rocket Nozzle Side Load Reduction Device. *Journal of Propulsion and Power*, **32**(6), 1395-1402.

9. Stark, R. & Génin, C. (2012). Experimental Study on Rocket Nozzle Side Load Reduction. *Journal of Propulsion and Power*, **28**(2), 307-311.